

Article

Analysis of Eigenfrequencies of a Circular Interface Delamination in Elastic Media Based on the Boundary Integral Equation Method

Mikhail V. Golub ^{*,†}  and Olga V. Doroshenko [†] 

Institute for Mathematics, Mechanics and Informatics, Kuban State University, 350040 Krasnodar, Russia; oldorosh@mail.ru

* Correspondence: m_golub@inbox.ru

† These authors contributed equally to this work.

Abstract: The widespread of composite structures demands efficient numerical methods for the simulation dynamic behaviour of elastic laminates with interface delaminations with interacting faces. An advanced boundary integral equation method employing the Hankel transform of Green's matrices is proposed for modelling wave scattering and analysis of the eigenfrequencies of interface circular partially closed delaminations between dissimilar media. A more general case of partially closed circular delamination is introduced using the spring boundary conditions with non-uniform spring stiffness distribution. The unknown crack opening displacement is expanded as Fourier series with respect to the angular coordinate and in terms of associated Legendre polynomials of the first kind via the radial coordinate. The problem is decomposed into a system of boundary integral equations and solved using the Bubnov-Galerkin method. The boundary integral equation method is compared with the meshless method and the published works for a homogeneous space with a circular open crack. The results of the numerical analysis showing the efficiency and the convergence of the method are demonstrated. The proposed method might be useful for damage identification employing the information on the eigenfrequencies estimated experimentally. Also, it can be extended for multi-layered composites with imperfect contact between sub-layers and multiple circular delaminations.

Keywords: elastic waves; boundary integral equation method; spring boundary conditions; laminate; delamination; eigenfrequency; diffraction; damage; resonance.



Citation: Golub, M.V.; Doroshenko O.V. Analysis of Eigenfrequencies of a Circular Interface Delamination in Elastic Media Based on the Boundary Integral Equation Method. *Mathematics* **2022**, *10*, 38. <https://doi.org/10.3390/math10010038>

Academic Editor: Nikolaos Tsitsas

Received: 30 November 2021

Accepted: 21 December 2021

Published: 23 December 2021

Publisher's Note: MDPI stays neutral with regard to jurisdictional claims in published maps and institutional affiliations.



Copyright: © 2021 by the authors. Licensee MDPI, Basel, Switzerland. This article is an open access article distributed under the terms and conditions of the Creative Commons Attribution (CC BY) license (<https://creativecommons.org/licenses/by/4.0/>).

1. Introduction

Widespread occurrence of composite structures in aerospace, aircraft, geophysics, building construction as well as in high-performance products led to the growth of the studies of the dynamics of various inhomogeneities or defects. Thus, crack analysis became a natural task for engineering applications due to the importance of the detection of defects and flaws known as delaminations. A special focus is on the interface delaminations, which detection is more cumbersome due to the additional reflections from the interface itself. If the faces of delaminations are partially closed, their identification becomes even more labour-consuming. In particular, the determination of the wave resonances and the eigenfrequencies or the natural frequencies has wide applications such as acoustic spectroscopy, prediction of possible structural failure and non-destructive testing. Indeed, wave propagation at the resonance frequencies exhibits itself in the larger resulting wave amplitudes and wave localization, which can be employed for determining the shape and properties of inhomogeneities using electromagnetic and acoustic waves [1]. Recently, local defect resonances were employed in the matters of non-destructive testing. For instance, inverse problems of the crack identification based on natural frequencies were studied theoretically and experimentally for rods [2,3] and plates [4,5].

From the mathematical point of view, wave resonances are related to the eigenfrequencies, the eigenvalues or the spectral points of the corresponding boundary-value problem, which naturally causes the wave energy capturing and localization or resonance blocking [6–11]. For the problems of analyzing wave resonances and scattering in an unbounded domain with inhomogeneities, the boundary integral equations method (BIEM) is among the most suitable, since the BIEM allows to employ Green's matrices constructed for unbounded media. Thus, analytical and semi-analytical methods, such as wave function expansion techniques [12], the ray theory and its modifications [13], the method of bi-characteristics [14] and various other methods, are restricted to the specific geometry or wavelengths. The purely numerical methods, e.g., the finite element method and the finite difference method, are not so efficient for modelling an unbounded media. This fact led to the development of novel hybrid methods, and a reasonable number of hybrid approaches are based on the BIEM [15]. Two valuable reviews on the BIEM with relevant references regarding numerical methods for determining the eigenvalues of elastodynamics problems based on the BIEM can be found in [15,16]. It should be also noted that the BIEM can also be efficiently applied for bounded domains: for example, Alves and Antunes [17] applied the method of fundamental solutions for calculating the elastic resonance frequencies and estimating the eigenmodes for the disk of some non-trivial shapes. Interface delaminations are often modelled as infinitesimally thin cuts with zero stresses on the crack faces, which corresponds to the open crack case. However, it might be significant to take into consideration that the crack faces are not fully open, and they are in contact without friction near the tips [18,19]. The interface delamination, in which the crack faces adjacent to the crack tips can interact, are also called bridged cracks [20]. The crack surfaces interaction can be modelled using the distributed spring model, which was introduced by Rice and Levy [21] and Baik and Thompson [22] for static and dynamic cases respectively, and it was experimentally validated recently in [23].

The BIEM is efficient for the solution of the scattering problem for strip-like [24–26], penny-shaped [24,27–35], elliptic [36], rectangular [37,38] arbitrary shaped [39] cracks. In the 1990s, location of the resonance poles or eigenfrequencies in the complex frequency plane for an elastic space was investigated for circular crack [40], elliptical crack [41] as well as rectangular and L-shaped cracks [38]. Boundary integral equations derived for a crack in a homogeneous space can be uncoupled into two equations, which is not possible for interface cracks between two dissimilar media. Apparently, for this reason, the properties of interface cracks have not been studied so extensively. As far as the authors know, the spectral properties of interface delaminations between dissimilar media and in the case of partial contact between the faces of a delamination has not been investigated in a three-dimensional case and the BIEM has not been yet extended to solve these problems.

This work aims to develop an efficient method for modelling a wide class of delaminations, which can be further used in hybrid methods (an example can be found in [42]) for structural health monitoring and nondestructive evaluation. The study presents the advanced BIEM based on the Fourier series expansion and the Hankel transform of Green's matrices suitable for the modelling wave scattering and the analysis of the eigenfrequencies of an partially closed circular interface delamination. The advanced BIEM extends previous BIEM implementations for circular cracks [28,29,40], where only an open crack and a uniform partially closed delamination [40] in a homogeneous space were considered. In this study, more general formulations based on the spring boundary conditions (SBCs) are employed, which allows for simulating partially closed delaminations with non-uniform partial contact between faces. Another novelty of the presented BIEM is in the consideration of interface delamination between two dissimilar media. The presented BIEM is compared with Krenk and Schmidt [28], Kundu and Boström [29] for a homogeneous space with circular delamination and the meshless method based on the BIEM [39] for dissimilar media. The results of the numerical analysis showing the efficiency of the method are demonstrated.

2. The Boundary Integral Equation Method

2.1. Formulation of the Problem

Let us consider steady-state harmonic motion of two dissimilar elastic isotropic half-spaces with an interface single delamination. The values related to the lower and upper half-spaces ($z \leq 0$) are denoted by indices 1 and 2 respectively. The harmonic multiplier $e^{-i\omega t}$ with angular frequency ω is conventionally omitted below. Material properties of each of the half-spaces V_j are defined by the mass density ρ_j , Poisson's ratio ν_j and Young's modulus E_j . The longitudinal and transverse wave velocities, respectively, take the form

$$c_{Lj} = \sqrt{\frac{E_j(\nu_j - 1)}{(2\nu_j - 1)(\nu_j + 1)\rho_j}}, \quad c_{Tj} = \sqrt{\frac{E_j}{2(\nu_j + 1)\rho_j}}. \tag{1}$$

Hereinafter, the index j indicating a half-space is omitted whenever possible.

In this study, a circular delamination Ω of radius a is addressed. Therefore, it is convenient to introduce a cylindrical coordinate system $x(r, \theta, z)$ as shown in Figure 1. The displacement vector $\mathbf{u} = \{u_r, u_\theta, u_z\}$ is expressed in terms of the potential functions ψ_1, ψ_2 and ψ_3 in the form

$$\begin{aligned} u_r &= \frac{\partial\psi_3}{\partial r} + \frac{\partial^2\psi_2}{\partial r\partial z} + \frac{1}{r} \frac{\partial\psi_1}{\partial\theta}, \\ u_\theta &= \frac{1}{r} \frac{\partial\psi_3}{\partial\theta} + \frac{1}{r} \frac{\partial^2\psi_2}{\partial\theta\partial z} - \frac{\partial\psi_1}{\partial r}, \\ u_z &= \frac{\partial\psi_3}{\partial z} - \left(\nabla^2 - \frac{\partial^2}{\partial z^2}\right)\psi_2, \end{aligned}$$

where

$$\nabla^2 = \frac{1}{r} \frac{\partial}{\partial r} + \frac{\partial^2}{\partial r^2} + \frac{1}{r^2} \frac{\partial^2}{\partial\theta^2} + \frac{\partial^2}{\partial z^2}.$$

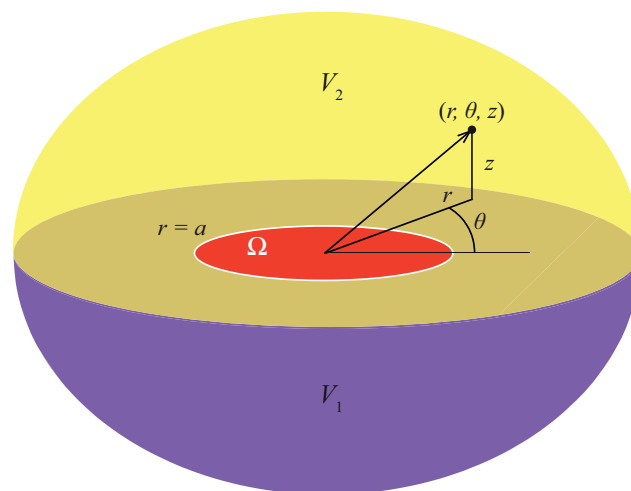


Figure 1. Statement of the problem.

The tangential and normal components (traction vector) of stress-tensor $\boldsymbol{\tau} = \{\sigma_{rz}, \sigma_{\theta z}, \sigma_{zz}\}$ are expressed in term of the components of the displacement vector \mathbf{u} as follows

$$\begin{aligned} \sigma_{rz} &= \frac{E}{2(\nu+1)} \left(\frac{\partial u_z}{\partial r} + \frac{\partial u_r}{\partial z} \right), \quad \sigma_{\theta z} = \frac{E}{2(\nu+1)} \left(\frac{1}{r} \frac{\partial u_z}{\partial\theta} + \frac{\partial u_\theta}{\partial z} \right), \\ \sigma_{zz} &= \frac{E}{(2\nu-1)(\nu+1)} \left((\nu-1) \frac{\partial u_z}{\partial z} + \nu \left(\frac{\partial u_r}{\partial r} + \frac{1}{r} u_r + \frac{1}{r} \frac{\partial u_\theta}{\partial\theta} \right) \right). \end{aligned}$$

In a cylindrical coordinate system, three governing equations of motion are three Helmholtz equations:

$$\nabla^2 \psi_3 + k_L^2 \psi_3 = 0, \quad \nabla^2 \psi_i + k_T^2 \psi_i = 0, \quad i = 1, 2. \tag{2}$$

written in terms of the wavenumbers of the longitudinal and transverse waves $k_p = \omega/c_p, p = T, L$ for each half-space. The continuity of the displacement and the traction vectors is assumed at the interface between two half-spaces except the delaminated zone Ω :

$$[\boldsymbol{\tau}](\mathbf{x}) = [\mathbf{u}](\mathbf{x}) = \mathbf{0}, \quad z = 0 \setminus \Omega. \tag{3}$$

Here square brackets $[f]$ denote an operator a jump of function f at the interface:

$$[f](\mathbf{x}) = \lim_{\delta \rightarrow 0} (f(r, \theta, z + \delta) - f(r, \theta, z - \delta)).$$

Since the considered interface damage Ω can be of various types (an open crack, a bridged crack or a partially closed crack), the SBCs are stated in the delaminated domain Ω :

$$\boldsymbol{\tau}^1(\mathbf{x}) = \boldsymbol{\tau}^2(\mathbf{x}) = \boldsymbol{\varkappa}(r) \cdot \Delta \mathbf{u}(\mathbf{x}), \quad \mathbf{x} \in \Omega. \tag{4}$$

Here $\Delta \mathbf{u}(\mathbf{x}) = \mathbf{u}_1(\mathbf{x}) - \mathbf{u}_2(\mathbf{x})$ is the crack opening displacement (COD) vector, $\boldsymbol{\varkappa}$ is three-by-three stiffness matrix, which is a function of the radial coordinate r .

Total wave-field in the media can be represented as a sum of an incident wave-field $\mathbf{u}^{in}(\mathbf{x})$ and the wave-field $\mathbf{u}^{sc}(\mathbf{x})$ scattered by the delamination Ω . In this paper, the solution method for an arbitrary incident wave-field is presented, but the numerical examples are demonstrated for the scattering of the incident plane waves incoming from the lower half-space.

2.2. Solution of an Auxiliary Problem for Each Half-Space

To construct the scattered wave-field, an auxiliary problem for an elastic half-space with a given surface load \mathbf{q} is considered, i.e.,

$$\boldsymbol{\tau}|_{z=0} = \mathbf{q}(r, \theta) = \{q_1, q_2, q_3\}.$$

The wave-fields excited by the surface load \mathbf{q} has an integral representation via the Green's matrix $\mathbf{k}(\mathbf{x}, \omega)$ and surface load [28,43], which are derived below using the Hankel transform and Fourier series expansion.

An integral representation of the wave-field can be constructed using expansion of the solution in the form of the Fourier series over the angular coordinate θ :

$$\begin{aligned} \psi_1(r, \theta, z) &= \sum_{m=0}^{\infty} \left(\psi_1^{1m}(r, z) \sin(m\theta) - \psi_1^{2m}(r, z) \cos(m\theta) \right), \\ \psi_2(r, \theta, z) &= \sum_{m=0}^{\infty} \left(\psi_2^{1m}(r, z) \cos(m\theta) + \psi_2^{2m}(r, z) \sin(m\theta) \right), \\ \psi_3(r, \theta, z) &= \sum_{m=0}^{\infty} \left(\psi_3^{1m}(r, z) \cos(m\theta) + \psi_3^{2m}(r, z) \sin(m\theta) \right) \end{aligned} \tag{5}$$

Since we deal with half-space, the limiting absorption principle is chosen for the uniqueness [44]. The substitution of (5) into (2) and the application the Hankel transform with respect to the radial coordinate r gives the following expansion coefficients for half-space

$$\begin{aligned}
 \psi_1^{nm}(r, z) &= \int_0^\infty \Psi_1^{nm}(\alpha) e^{-\gamma_2|z|} J_m(\alpha r) \alpha \, d\alpha, \\
 \psi_2^{nm}(r, z) &= \int_0^\infty \Psi_2^{nm}(\alpha) e^{-\gamma_2|z|} J_m(\alpha r) \alpha \, d\alpha, \\
 \psi_3^{nm}(r, z) &= \int_0^\infty \Psi_3^{nm}(\alpha) e^{-\gamma_1|z|} J_m(\alpha r) \alpha \, d\alpha,
 \end{aligned}
 \tag{6}$$

where conditions $\text{Im } \gamma_n \geq 0, \text{Re } \gamma_n \leq 0$ must be satisfied for $\gamma_1 = \sqrt{\alpha^2 - k_L^2}, \gamma_2 = \sqrt{\alpha^2 - k_T^2}$ and functions Ψ_i^{nm} are determined from the boundary conditions on the surface $z = 0$.

Following [28,45], the displacement and the traction vectors can also be expanded into Fourier series:

$$\begin{aligned}
 \mathbf{u}(r, \theta, z) &= \sum_{n=1}^2 \sum_{m=0}^\infty \mathbf{Y}^{nm}(\theta) \mathbf{u}^{nm}(r, z), \\
 \boldsymbol{\tau}(r, \theta, z) &= \sum_{n=1}^2 \sum_{m=0}^\infty \mathbf{Y}^{nm}(\theta) \boldsymbol{\tau}^{nm}(r, z),
 \end{aligned}
 \tag{7}$$

written in terms of diagonal matrices:

$$\begin{aligned}
 \mathbf{Y}^{1m}(\theta) &= \text{diag}\{\cos(m\theta), \sin(m\theta), \cos(m\theta)\}, \\
 \mathbf{Y}^{2m}(\theta) &= \text{diag}\{\sin(m\theta), -\cos(m\theta), \sin(m\theta)\},
 \end{aligned}$$

and the expansion coefficients:

$$\begin{aligned}
 u_r^{nm}(r, z) &= \frac{\partial \psi_3^{nm}(r, z)}{\partial r} + \frac{\partial^2 \psi_2^{nm}(r, z)}{\partial r \partial z} + \frac{m}{r} \psi_1^{nm}(r, z), \\
 u_\theta^{nm}(r, z) &= -\frac{m}{r} \left(\psi_3^{nm}(r, z) + \frac{\partial \psi_2^{nm}(r, z)}{\partial z} \right) - \frac{\partial \psi_1^{nm}(r, z)}{\partial r},
 \end{aligned}$$

which are expressed via functions (6). Using recurrent formulae for the Bessel functions:

$$\left(\frac{\partial}{\partial r} + \frac{m}{r} \right) J_m(\alpha r) = \alpha J_{m-1}(\alpha r), \quad \left(\frac{\partial}{\partial r} - \frac{m}{r} \right) J_m(\alpha r) = -\alpha J_{m+1}(\alpha r),$$

the following integral representations for all the potentials can be obtained

$$\begin{aligned}
 \left(\frac{\partial}{\partial r} + \frac{m}{r} \right) \psi_i^{nm}(r, z) &= \int_0^\infty \Psi_i^{nm}(\alpha) e^{-\gamma|z|} \alpha J_{m-1}(\alpha r) \alpha \, d\alpha, \\
 \left(\frac{\partial}{\partial r} - \frac{m}{r} \right) \psi_i^{nm}(r, z) &= -\int_0^\infty \Psi_i^{nm}(\alpha) e^{-\gamma|z|} \alpha J_{m+1}(\alpha r) \alpha \, d\alpha.
 \end{aligned}$$

For the Fourier series expansion coefficients in (7) one can obtain the following relations

$$\begin{aligned}
 (u_r^{nm} + u_\theta^{nm})(r, z) &= \left(\frac{\partial}{\partial r} - \frac{m}{r} \right) \left(\psi_3^{nm}(r, z) + \frac{\partial \psi_2^{nm}(r, z)}{\partial z} - \psi_1^{nm}(r, z) \right), \\
 (u_r^{nm} - u_\theta^{nm})(r, z) &= \left(\frac{\partial}{\partial r} + \frac{m}{r} \right) \left(\psi_3^{nm}(r, z) + \frac{\partial \psi_2^{nm}(r, z)}{\partial z} + \psi_1^{nm}(r, z) \right), \\
 (\tau_{rz}^{nm} + \tau_{\theta z}^{nm})(r, z) &= \frac{E}{2(\nu + 1)} \left(\frac{\partial u_z^{nm}}{\partial r} + \frac{1}{r} \frac{\partial u_z^{nm}}{\partial \theta} + \frac{\partial u_r^{nm}}{\partial z} + \frac{\partial u_\theta^{nm}}{\partial z} \right)
 \end{aligned}$$

$$(\tau_{rz}^{nm} - \tau_{\theta z}^{nm})(r, z) = \frac{E}{2(\nu + 1)} \left(\frac{\partial u_z^{nm}}{\partial r} - \frac{1}{r} \frac{\partial u_r^{nm}}{\partial \theta} + \frac{\partial u_r^{nm}}{\partial z} - \frac{\partial u_\theta^{nm}}{\partial z} \right).$$

Accordingly, it makes sense to introduce the following vectors

$$\begin{aligned} \hat{\mathbf{u}}^{nm}(r, z) &= \{u_r^{nm} + u_\theta^{nm}, u_r^{nm} - u_\theta^{nm}, u_z^{nm}\}, \\ \hat{\boldsymbol{\tau}}^{nm}(r, z) &= \{\tau_{rz}^{nm} + \tau_{\theta z}^{nm}, \tau_{rz}^{nm} - \tau_{\theta z}^{nm}, \tau_{zz}^{nm}\}. \end{aligned} \tag{8}$$

Further, it is natural to represent also the traction vector $\mathbf{q}(r, \theta)$ in the form of a Fourier series expansion as

$$\mathbf{q}(r, \theta) = \sum_{m=0}^{\infty} \sum_{n=1}^2 \mathbf{Y}^{nm}(\theta) \cdot \mathbf{q}^{nm}(r),$$

and construct

$$\hat{\mathbf{q}}^{nm}(r) = \{q_1^{nm}(r) + q_2^{nm}(r), q_1^{nm}(r) - q_2^{nm}(r), q_3^{nm}(r)\}$$

from the expansion coefficients.

Finally, the integral representation of the wave-fields in each half-space excited by an arbitrary surface load is written

$$\hat{\mathbf{u}}_j^{\text{sc}, nm}(r, z) = \int_{\Gamma} \mathbf{J}^m(\alpha r) \cdot \mathbf{K}_j(\alpha, z) \cdot \hat{\mathbf{Q}}^{nm}(\alpha) \alpha \, d\alpha, \tag{9}$$

where the matrix $\mathbf{J}^m(\alpha r) = \text{diag}\{J_{m+1}(\alpha r), J_{m-1}(\alpha r), J_m(\alpha r)\}$ is the diagonal matrix of Bessel functions and the Hankel transform $\hat{\mathbf{Q}}^{nm}$ of the expansion coefficients for the surface load $\hat{\mathbf{q}}^{nm}$ also has an integral representation:

$$\hat{\mathbf{Q}}^{nm}(\alpha) = \int_0^{\infty} \mathbf{J}^m(\alpha r) \cdot \hat{\mathbf{q}}^{nm}(r) r \, dr.$$

The Hankel transform of Green’s matrix $\hat{\mathbf{K}}_j(\alpha, z)$ for the rearranged traction vector $\hat{\mathbf{q}}$ is constructed in the same manner as in [46], but in cylindrical coordinates, see [35] for more details.

2.3. Solution of the Boundary Integral Equation

Next, the solutions for two auxiliary problems for each half-space are employed to formulate the boundary integral equation for the delamination occupying domain Ω . Thus, the Hankel transforms of the components of the traction vector at the common interface between two half-spaces can be expressed in terms of the Hankel transform of an unknown displacement jump $\Delta \hat{\mathbf{u}}^{nm}$:

$$\hat{\mathbf{Q}}^{nm}(\alpha) = [\hat{\mathbf{K}}_1(\alpha, 0) - \hat{\mathbf{K}}_2(\alpha, 0)]^{-1} \Delta \hat{\mathbf{u}}^{nm}(\alpha) = \hat{\mathbf{L}}(\alpha) \cdot \Delta \hat{\mathbf{u}}^{nm}(\alpha).$$

In the case of delamination, the latter is the crack opening displacement (COD).

Substitution of the integral representations of the scattered wave-fields (9) into the boundary conditions (3) and (4) leads to the boundary integral equation:

$$\int_0^{\infty} \mathbf{J}^m(\alpha r) \cdot \hat{\mathbf{L}}(\alpha) \cdot \Delta \hat{\mathbf{u}}^{nm}(\alpha) d\alpha - \boldsymbol{\varkappa}(r) \cdot \Delta \hat{\mathbf{u}}^{nm}(r) = -\hat{\boldsymbol{\tau}}^{\text{in}, nm}(r), \quad r \leq a. \tag{10}$$

Following [28,29,45], the COD is expanded in terms of associated Legendre polynomials of the first kind P_k^m

$$\Delta \hat{\mathbf{u}}^{nm}(r) = \sum_{k=0}^{\infty} \boldsymbol{\phi}_k^m(r) c_k^{nm}.$$

Here diagonal matrices

$$\begin{aligned} \boldsymbol{\phi}_k^m(r) &= \text{diag}\{\phi_{1k}^m(r), \phi_{2k}^m(r), \phi_{3k}^m(r)\}, \\ \phi_{1k}^m(r) &= \frac{P_{m+2k+2}^{m+1}(\sqrt{1-r^2/a^2})}{P_{m+2k+2}^{m+2}(0)}, \quad \phi_{2k}^m(r) = \frac{P_{m+2k}^{m-1}(\sqrt{1-r^2/a^2})}{P_{m+2k}^m(0)}, \\ \phi_{3k}^m(r) &= \frac{P_{m+2k+1}^m(\sqrt{1-r^2/a^2})}{P_{m+2k+1}^{m+1}(0)} \end{aligned}$$

are introduced for brevity. It should be mentioned that due to the properties of associated Legendre polynomials, an amendment in the indices is required for $m = 0$:

$$\begin{aligned} \phi_{1k}^0(r) &= \frac{P_{2k+2}^1(\sqrt{1-r^2/a^2})}{P_{2k+2}^2(0)}, \quad \phi_{2k}^0(r) = \phi_{1k}^0(r), \\ \phi_{3k}^0(r) &= \frac{P_{2k+1}^0(\sqrt{1-(r/a)^2})}{P_{2k+1}^1(0)}. \end{aligned}$$

The Hankel transforms $\Phi_{1k}^m(\alpha a)$ of the basis functions $\phi_{1k}^m(r)$ are expressed in terms of Bessel functions J_m . Taking into account the equality $J_{-1} = -J_1$, the following relations can be obtained for $m = 0$

$$\begin{aligned} \Phi_{1k}^0(\alpha a) &= \int_0^a \phi_{1k}^0(r) J_1(\alpha r) r dr = (-1)^k \sqrt{\frac{\pi a}{2}} \frac{J_{2k+5/2}(\alpha a)}{\alpha^{3/2}}, \\ \Phi_{2k}^0(\alpha a) &= \int_0^a \phi_{1k}^0(r) J_{-1}(\alpha r) r dr = -\Phi_{1k}^0(\alpha a), \\ \Phi_{3k}^0(\alpha a) &= \int_0^a \phi_{3k}^0(r) J_0(\alpha r) r dr = (-1)^k \sqrt{\frac{\pi a}{2}} \frac{J_{2k+3/2}(\alpha a)}{\alpha^{3/2}}, \end{aligned}$$

and for $m \geq 1$

$$\begin{aligned} \Phi_{1k}^m(\alpha a) &= \int_0^a \phi_{1k}^m(r) J_{m+1}(\alpha r) r dr = (-1)^k \sqrt{\frac{\pi a}{2}} \frac{J_{m+2k+5/2}(\alpha a)}{\alpha^{3/2}}, \\ \Phi_{2k}^m(\alpha a) &= \int_0^a \phi_{2k}^m(r) J_{m-1}(\alpha r) r dr = (-1)^k \sqrt{\frac{\pi a}{2}} \frac{J_{m+2k+1/2}(\alpha a)}{\alpha^{3/2}}, \\ \Phi_{3k}^m(\alpha a) &= \int_0^a \phi_{3k}^m(r) J_m(\alpha r) r dr = (-1)^k \sqrt{\frac{\pi a}{2}} \frac{J_{m+2k+3/2}(\alpha a)}{\alpha^{3/2}}. \end{aligned}$$

The employment of the Bubnov-Galerkin scheme allows discretizing the system of boundary integral Equation (10):

$$\sum_{k=0}^{\infty} (\mathbf{A}_{kk'}^{m,L} + \mathbf{A}_{kk'}^{m,\varkappa}) \cdot \mathbf{c}_k^{nm} = \mathbf{g}_{k'}^{nm}, \quad m = 0, 1, 2, \dots \tag{11}$$

$$\mathbf{A}_{kk'}^{m,L} = \int_0^{\infty} \boldsymbol{\Phi}_{k'}^m(\alpha) \cdot \hat{\mathbf{L}}(\alpha) \cdot \boldsymbol{\Phi}_k^m(\alpha) \alpha d\alpha,$$

$$\mathbf{A}_{kk'}^{m,\varkappa} = - \int_0^a \boldsymbol{\phi}_{k'}^m(r) \cdot \varkappa(r) \cdot \boldsymbol{\phi}_k^m(r) r dr,$$

$$\mathbf{g}_{k'}^{nm} = - \int_0^a \boldsymbol{\phi}_{k'}^m(r) \cdot \boldsymbol{\tau}^{\text{in},nm}(r) r dr.$$

Here $\Phi_k^m(\alpha)$ is the Hankel transform of the matrix $\phi_k^m = \{\phi_{1k}^m, \phi_{2k}^m, \phi_{3k}^m\}$, the first term in the right-hand side $\mathbf{A}_{kk'}^{m,L}$ describe the behaviour of an open crack, whereas the second term $\mathbf{A}_{kk'}^{m,\varkappa}$ takes into account the interaction of the faces of the delamination modelled employing the distributed spring with stiffness $\varkappa(r)$.

Using discretized form (11) of boundary integral Equation (10), one can write that the eigenfrequencies $\hat{\omega}$ satisfy one of the following equations:

$$\det \left[\mathbf{A}_{kk'}^{m,L}(\hat{\omega}) + \mathbf{A}_{kk'}^{m,\varkappa}(\hat{\omega}) \right] = 0, \quad m = 0, 1, 2, \dots$$

Therefore, the eigenfrequencies of circular interface delaminations can be separated into different classes in accordance with the order m of the trigonometric functions in series (5). Accordingly, the eigenfrequencies $\hat{\omega}_n^m$ are enumerated using two indices. For simplicity, the normalized eigenfrequencies $\hat{k}_n^m = \hat{\omega}_n^m a / c_{T1}$ are employed further.

2.4. Far-Field Asymptotic

The direct calculation of the scattered wave-field $\hat{u}_j^{sc, nm}(r, z)$ in the form of (9) gives significant oscillation due to the behaviour of the integrand. Besides, it is also necessary to take into account the integral contours. On the other hand, asymptotic representations of the scattered wave-fields in the far-field zone can be determined considering the contribution of stationary points into the values of the oscillating integrals [39]. An introduction of spherical coordinates is preferable for constructing the far-field asymptotics:

$$r = R \sin \vartheta, \quad \theta = \vartheta, \quad z = R \cos \vartheta,$$

where $0 \leq \vartheta \leq \frac{\pi}{2}$ corresponds to the upper half-space, and $-\frac{\pi}{2} \leq \vartheta \leq 0$ corresponds to the lower half-space. The oscillation of the integrand in (10) grows with R increases, which greatly complicates the calculation of integrals. The dominating integral function of the form $e^{i\omega RC}$ can be explicitly distinguished by the asymptotic method. For this, it is required to determine the contribution of critical points into the asymptotic of the oscillating integrals, which includes stationary points of the exponents (phase function), poles and branching points.

The displacement vector for the circular crack in the spherical coordinates is rewritten as follows:

$$\mathbf{u}(R, \theta, \vartheta) = \sum_{n=1}^2 \sum_{m=0}^{\infty} \mathbf{Y}^{nm}(\theta) \cdot \mathbf{C}^{-1} \cdot \hat{\mathbf{u}}^{nm}(R, \vartheta), \tag{12}$$

where

$$\mathbf{C} = \begin{pmatrix} 1 & 1 & 0 \\ 1 & -1 & 0 \\ 0 & 0 & 1 \end{pmatrix}$$

is the transfer matrix for the rearranged displacement vector in (8). If the decomposition of the Hankel transform of Green's matrices $\hat{\mathbf{K}}_j$ for the media $z \gtrless 0$ in the form

$$\hat{\mathbf{K}}_j(\alpha, z) = \sum_{p=1}^2 \hat{\mathbf{K}}_{pj}(\alpha) e^{-\gamma_{pj}|z|},$$

is substituted into (9), the following expression for (12) can be deduced:

$$\mathbf{u}(R, \theta, \vartheta) = \sum_{j=1}^2 \mathbf{u}_j(R, \theta, \vartheta) = \sum_{j=1}^2 \sum_{n=1}^2 \sum_{m=0}^{\infty} \mathbf{Y}^{nm}(\theta) \cdot \mathbf{C}^{-1} \cdot \hat{\mathbf{u}}_j^{nm}(R, \vartheta). \tag{13}$$

Here, $u_j(R, \theta, \vartheta)$ describes scattered longitudinal ($j = 1$) and transverse ($j = 2$) waves in terms of integral representations

$$\hat{u}_j^{nm}(R, \vartheta) = \sum_{p=1}^2 \int_{\Gamma} \mathbf{J}^m(\alpha R \sin \vartheta) \cdot \hat{\mathbf{K}}_{pj}(\alpha) \cdot \hat{\mathbf{L}}(\alpha) \cdot \Delta \hat{\mathbf{U}}^{nm}(\alpha) e^{-\gamma_{pj} R |\cos \vartheta|} \alpha d\alpha. \tag{14}$$

In integral representation (14), the explicit dependence on α has the form

$$e^{-\gamma_{pj} R |\cos \vartheta|} = e^{(-1)^{(j+1)} i R \cos \vartheta \sqrt{k_p^2 - \alpha^2}}.$$

The integration contour Γ^+ can be split up into two parts for each term in (14): $D_{pj} = \{|\alpha| < k_{pj}\} \cap \Gamma^+$ and Γ^+ / D_{pj} . In D_{pj} , the exponential $e^{-\gamma_{pj} R |\cos \vartheta|}$ becomes purely imaginary, whereas it is purely real outside D_{pj} . Since the contribution of limiting points in the values of the integrals (14) decay faster than $O(R^{-1})$, it is enough to apply the method of stationary phase [47]. Thus, the phase functions

$$s_1(\alpha) = \alpha \sin \vartheta - (-1)^j \cos \vartheta \sqrt{k_p^2 - \alpha^2},$$

$$s_2(\alpha) = -\alpha \sin \vartheta - (-1)^j \cos \vartheta \sqrt{k_p^2 - \alpha^2}$$

have stationary points $\alpha_{pj} = k_{pj} \sin \vartheta$. Using the relation between Bessel function and Hankel functions of the first and the second kind (H_k^1 and H_k^2) and their asymptotic representations at $R \rightarrow \infty$ [48]:

$$J_k(R) = \frac{1}{2} (H_k^1(R) + H_k^2(R)) \approx \frac{1}{\sqrt{2\pi R}} \left(e^{i(R - \frac{k\pi}{2} - \frac{\pi}{4})} + e^{-i(R - \frac{k\pi}{2} - \frac{\pi}{4})} \right),$$

the contribution of nondegenerate stationary points α_{pj} into the asymptotics of the integrals as $R \rightarrow \infty$ can be determined. According to the stationary phase method [47], the dominant term of the asymptotics of \hat{u}^{nm} given by (12) in the far-field zone ($R \gg 1$) has the form

$$\hat{u}_j^{nm}(R, \vartheta) \approx \sum_{p=1}^2 \mathbf{b}_{pj}^{nm}(\theta, \vartheta) e^{iRk_{pj} / R},$$

where

$$\mathbf{b}_{pj}^{nm}(\theta, \vartheta) = |\cos \vartheta| k_{pj} \hat{\mathbf{J}}^m \cdot \hat{\mathbf{K}}_j(\alpha_{pj}) \cdot \hat{\mathbf{L}}(\alpha_{pj}) \cdot \Delta \hat{\mathbf{U}}(\alpha_{pj}),$$

$$\hat{\mathbf{J}}^m = \text{diag} \left\{ e^{-i\pi(m+1)/2}, e^{-i\pi(m+1)/2}, e^{-i\pi m/2} \right\}.$$

3. Convergence and Comparison

The advanced BIEM code has been implemented in Fortran 90 and numerically validated (see Sections 3.1 and 3.2). Properties of the materials used further for the numerics are given in Table 1. In the case of a homogeneous space, glass is chosen to compare with [28,29,40]. If two dissimilar half-spaces are considered, then the lower half-space has material properties of aluminium and the upper half-space has properties of polycarbonate.

Table 1. Material properties.

Material	Young’s Modulus E_r GPa	Poisson’s Ratio, ν	Density, ρ , kg/m ³
Glass	69.15	0.25	2770
Aluminium	70	0.33	2700
Polycarbonate	2.38	0.36	1200

Components of the diagonal spring stiffness matrix \varkappa used in the SBCs can be chosen differently, e.g., following [31,49,50], where the ratios between normal and tangential

stiffnesses were estimated. However, since the study focuses on the numerical aspects of the BIEM for partially delaminated zones, the equality of the three components of the stiffness matrix has been assumed for the numerics below:

$$\varkappa(r) = \kappa(r)\mathbf{I}_3.$$

The proposed BIEM allows to simulate arbitrarily distributed spring stiffness, for the numerical analysis spring stiffness defined via the following representation has been chosen

$$\kappa(r) = \begin{cases} \kappa^0 & r < a - 2\Delta a \\ \kappa^0 + \frac{\kappa^{\text{tip}} - \kappa^0}{2} \cdot \left(\frac{r - a + 2\Delta a}{\Delta a}\right)^2 & a - 2\Delta a < r < a - \Delta a \\ \kappa^{\text{tip}} + \frac{\kappa^0 - \kappa^{\text{tip}}}{2} \cdot \left(\frac{a - r}{\Delta a}\right)^2 & a - \Delta a < r < a \end{cases}$$

The latter allows to investigate four kinds of delaminations, which are assumed as the most natural [51]: an open crack, a bridged crack, a uniformly partially closed delamination and a bridged delamination. In a generalized case of a bridged delamination ($\Delta a \neq 0$ and $\kappa^0 \neq \kappa^{\text{tip}}$), while for three other types some conditions are assumed. The typical plots for the all four cases are shown in Figure 2 and the conditions for the considered type of cracks are listed in Table 2.

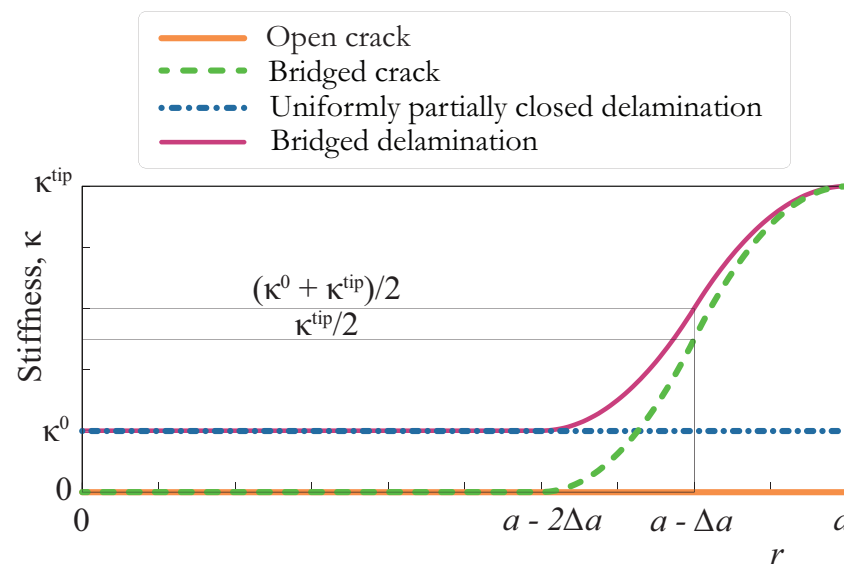


Figure 2. Stiffness variation for four kinds of delamination under consideration.

Table 2. The characteristics of four kinds of delaminations considered in the study.

Open Crack	Bridged Crack	Uniformly Partially Closed Delamination	Bridged Delamination (the Most General Case)
$\kappa^0 = \kappa^{\text{tip}} = 0$ $\Delta a = 0$	$\kappa^0 = 0, \kappa^{\text{tip}} \neq 0$ $\Delta a \neq 0$	$\kappa^0 = \kappa^{\text{tip}} \neq 0$ $\Delta a = 0$	$\kappa^0 \neq \kappa^{\text{tip}}$ $\Delta a \neq 0$

3.1. Crack Opening Displacement and Wave-Fields

First, the presented BIEM has been compared with the results obtained by Kundu and Boström [29] and Krenk and Schmidt [28]. Figure 3 depicts the amplitudes of the COD vector $|\Delta u|$ for an open circular crack in a homogeneous glass space induced by for the normally incident longitudinal wave at $k_T a = 10$. This figure illustrates a good agreement of the presented BIEM with the meshless method [39] and the results of [29], which are also shown in Figure 3. The far-field asymptotic can also be validated via the comparison

with [28], where a homogeneous space was considered. Figure 4 exhibits the amplitudes $|u_j(10^3, \theta = \pi/2 \pm \pi/2, \vartheta)|R/a^2$, i.e., in the plane x_1Ox_3 , and a very good coincidence with the results obtained by Krenk and Schmidt [28] is observed for $R/a > 10$. In Figure 4, value $R/a = 10^3$ has been used, while it should be mentioned that the results are almost the same for $R/a > 10$ due to the same normalization.

Two more examples of the comparison of the presented advanced BIEM with the meshless method [39] for circular delaminations are exhibited in Figures 5 and 6. In these figures, two contour plots show the vertical components of the COD $|\Delta u_3(x_1, x_2)|$ of a circular open crack calculated using the present BIEM and the meshless approach [39] in the case of the incident the SV-wave at 30° angle to plane $x_3 = 0$ and 90° angle to plane $x_2 = 0$ for homogeneous glass (Figure 5) and for aluminium/polycarbonate (Figure 6) at $k_{T2}a = 20$. The meshless method [39] gives an integral estimation of the COD, which allows achieving a good convergence for the solution in a far-field zone or the average COD, but it leads to a slow convergence for the COD itself. Therefore, the proposed advanced BIEM provides a more accurate solution with lower computational costs for the COD compared to the meshless method [39].

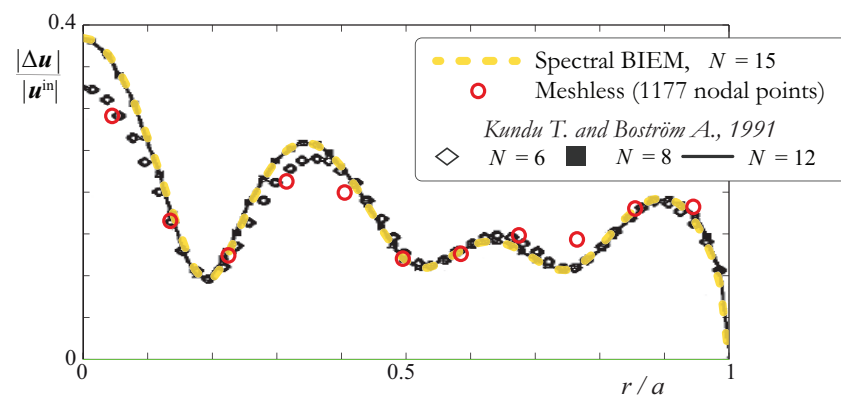


Figure 3. Amplitudes of the COD $|\Delta u|$ of an open circular crack in the elastic space with Poisson’s ratio $\nu = 0.25$ for the normally incident longitudinal wave at $k_{T2}a = 10$: comparison with [29].

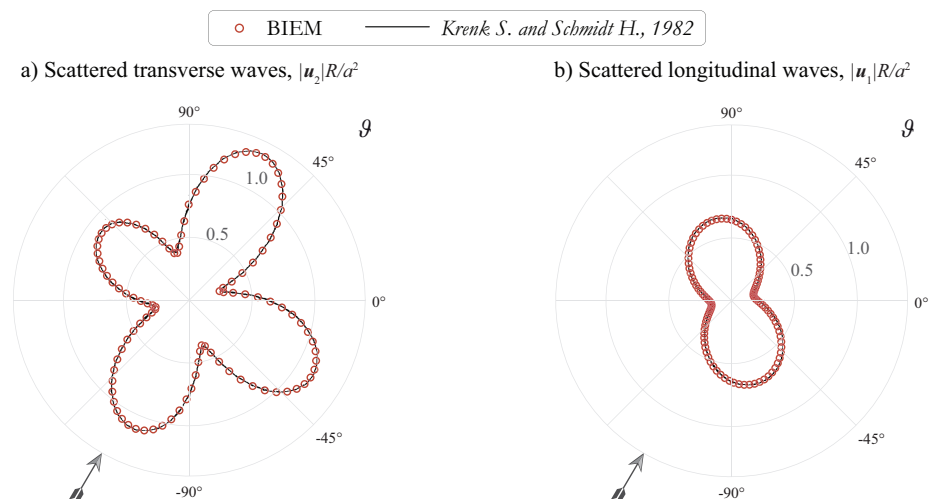


Figure 4. Amplitudes of transverse $|u_2(10^3, \theta = \pi/2 \pm \pi/2, \vartheta)|$ (a) and longitudinal $|u_1(10^3, \theta = \pi/2 \pm \pi/2, \vartheta)|$ (b) waves scattered by an open circular crack in the elastic space (glass) for the obliquely incident transverse SV-wave (incidence angle 30° to the plane $x_3 = 0$ and 90° angle to plane $x_2 = 0$ at $k_{T2}a = 2$. Comparison with [28].

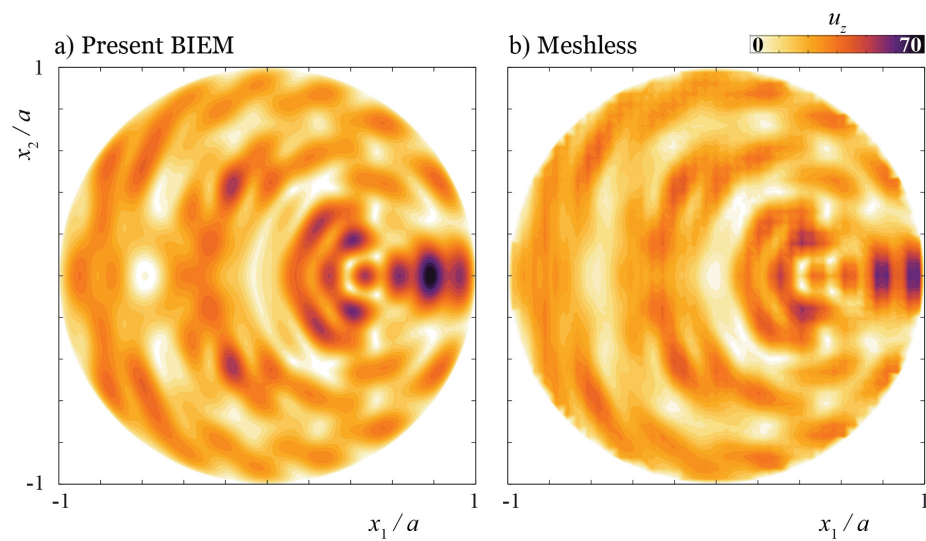


Figure 5. Amplitudes of the vertical components of the COD $|\Delta u_3(x_1, x_2)|$ of a circular open crack calculated using the present BIEM and the meshless approach [39] for the transverse wave incident at 30° angle to plane $x_3 = 0$ and 90° angle to plane $x_2 = 0$: space made of glass, $k_{T2}a = 20$.

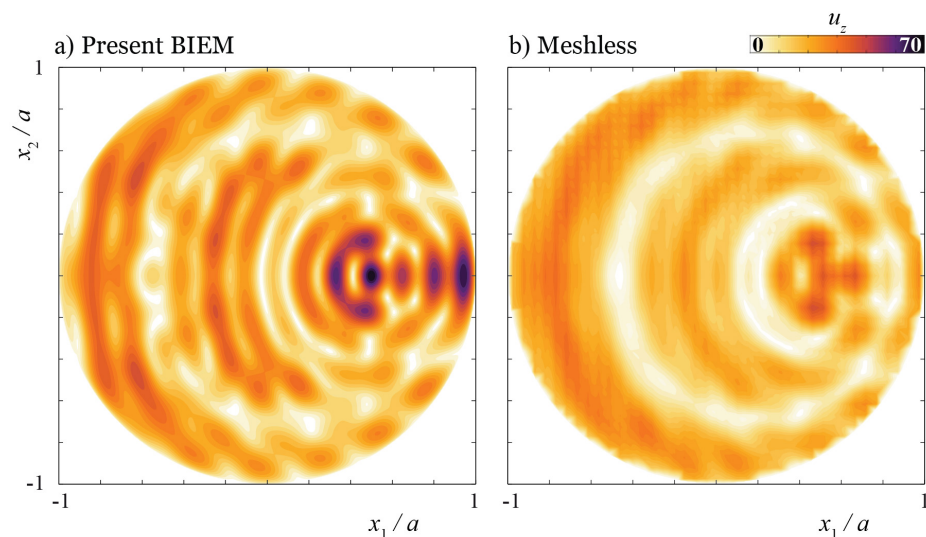


Figure 6. Amplitudes of the vertical components of the COD $|\Delta u_3(x_1, x_2)|$ of a circular open crack calculated using the present BIEM and the meshless approach [39] for the transverse wave incident at 30° angle to plane $x_3 = 0$ and 90° angle to plane $x_2 = 0$: two half-spaces made of aluminium and polycarbonate, $k_{T2}a = 20$.

Figure 7, where the amplitudes of the COD vector $|\Delta \mathbf{u}(x_1, 0)|$ for the same parameters as in Figure 6 are shown, demonstrates that the BIEM has rather fast convergence for all kinds of delaminations under study. A fast convergence rate is provided by diagonal dominance in the left-hand side matrix, which becomes stronger if $\kappa \neq 0$. Figure 7 also illustrates the fact that scattering by a uniformly partially closed delamination and bridged delamination is rather similar.

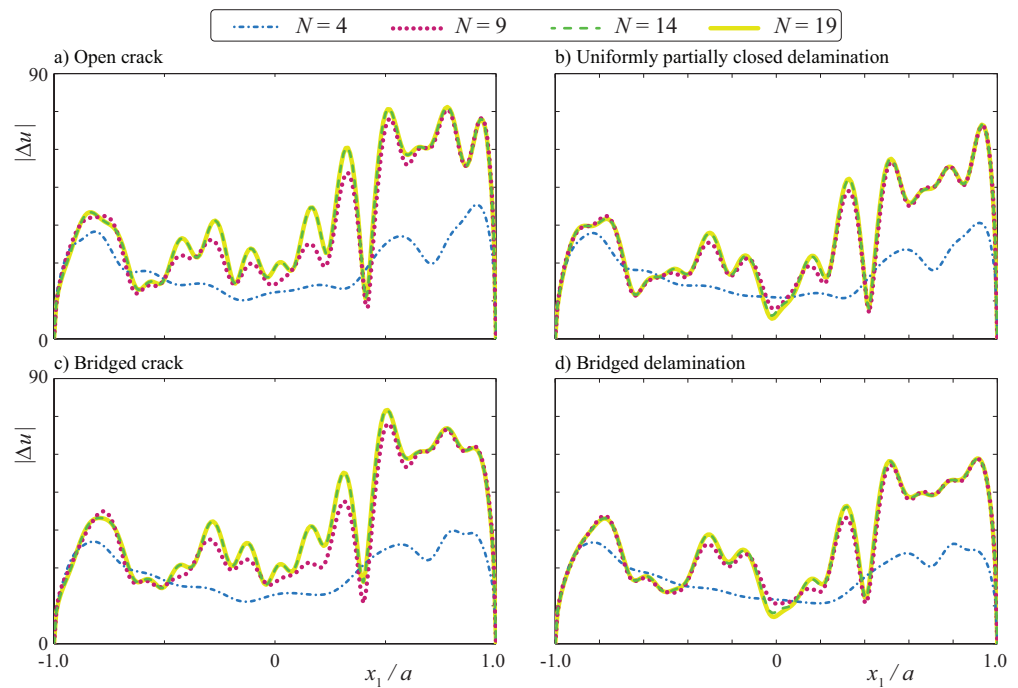


Figure 7. Amplitudes of the COD $|\Delta u(x_1, 0)|$ of circular delaminations for a transverse wave incident at 30° angle to plane $x_3 = 0$ and 90° angle to plane $x_2 = 0$: two half-spaces made of aluminium and polycarbonate, $k_{T2}a = 20$.

3.2. Eigenfrequencies

The eigenfrequencies of an open circular crack in the homogeneous space made of glass calculated by the present BIEM have been compared with [41], where the first three eigenfrequencies were computed using Padé approximations: the results of comparison are given in Table 3. In this table, three decimal places are given to compare with [41]. It should be also noted that due to different introduction of the Fourier transform, the real and imaginary parts of the eigenfrequencies calculated in this study and by Kaptsov and Shifrin [41] change places.

Analysis of a partial contact between faces of delamination can be provided using Figure 8, where trajectories of the eigenfrequencies $\hat{k}_n^m(\kappa)$ of a circular uniformly distributed delamination in an elastic space made of glass in the frequency complex plane are depicted. Markers show the eigenfrequencies for intermediate values of $\kappa a / \hat{\mu}$ ($\hat{\mu} = \mu_2$ is the shear modulus of the upper half-space). The obtained spectral points \hat{k}_n are also in agreement with results obtained by Eriksson [40].

Table 3. Eigenfrequencies \hat{k}_n^0 of an open crack in a homogeneous space (glass): comparison with [41].

The Present BIEM	Padé Approximations [41]
1.639–0.595 i	1.639–0.595 i
4.394–0.658 i	4.351–0.713 i
2.445–3.786 i	2.308–3.850 i

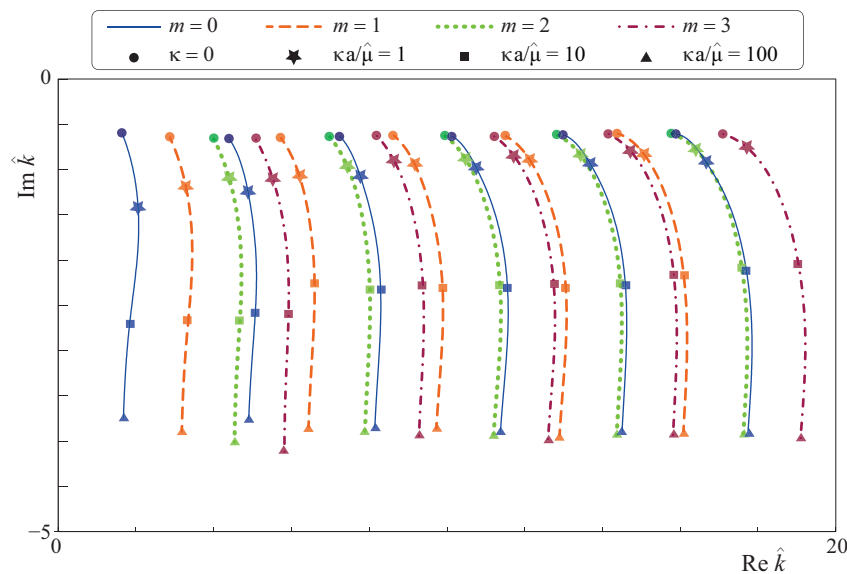


Figure 8. Eigenfrequencies $\hat{k}_n^m(\kappa)$ of a circular uniformly distributed delamination in the elastic space made of glass.

4. Resonance Frequencies and Wave Scattering

4.1. Open Crack

At first, an elastic space with an open crack is considered. Figure 9 shows the variation of the values of real and imaginary parts of the eigenfrequencies \hat{k}_n^m with the increase of Poisson’s ratio of elastic space. Markers of larger radius in Figure 9 correspond to larger values of Poisson’s ratio, whereas the eigenfrequencies are given for the first four groups and the first five modes, respectively. One can see that the eigenfrequencies are more or less uniformly distributed along $Im\hat{k} = 0$ axis (see also Figure 8) and that the larger ν the larger $Re\hat{k}_n^m$. The smallest attenuation, which is given as the imaginary part of the eigenfrequency $Im\hat{k}_n^m$ is achieved at $\nu = 0$ for the majority of cases. At the same time, the largest attenuation is usually observed in the vicinity of $\nu = 0.4$, and the attenuation decreases with the increase of Poisson’s ratio for $\nu > 0.4$. The latter might be related with the sufficient increase of the ratio

$$\beta = c_{Lj}/c_{Tj} = \sqrt{\frac{2(\nu_j - 1)}{2\nu_j - 1}}$$

between transverse and longitudinal velocities (1) with the increase of Poisson’s ratio if $\nu > 0.4$: $\beta_j(\nu = 0.35) = 1.472$, $\beta_j(\nu = 0.4) = 1.732$ and $\beta_j(\nu = 0.45) = 2.345$.

A similar analysis can also be performed for an open circular crack between two dissimilar materials. The case of dissimilar half-spaces is even more complicated for the analysis due to extra reflection by the interface itself and additional parameters (material properties of the second media) to be taken into account. As an example, Figure 10 shows the eigenfrequencies $\hat{k}_n^0(\nu_1, \nu_2)$ for a circular crack between dissimilar elastic half-spaces with identical densities ($\rho_1 = \rho_2$) and shear moduli ($\mu_1 = \mu_2$). In this case, an increase of any of Poisson’s ratios also leads to the increase of the real part of eigenfrequencies $Re\hat{k}_n^m$. It should be also mentioned that trajectories of \hat{k}_n^m do not change their behaviour qualitatively in the case of dissimilar media.

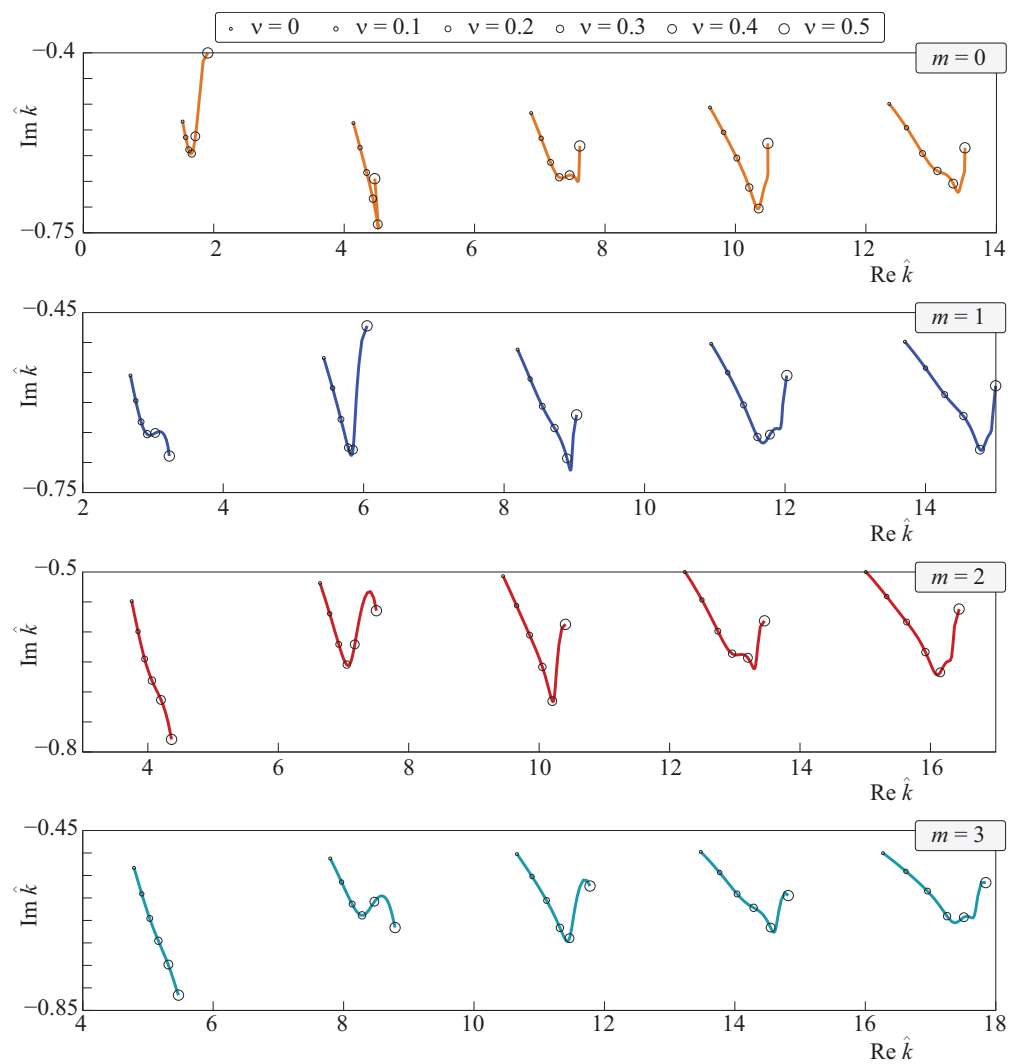


Figure 9. Eigenfrequencies \hat{k}_n^m for a circular crack in an elastic space with Poisson ratio ν .

4.2. Partially Closed Delamination

In this subsection, the eigenfrequencies and eigenforms of various circular delaminations are compared and analysed. The values of the first five eigenfrequencies \hat{k}_1^0 of circular delaminations of the four kinds considered in the study are given in Tables 4–7. Tables 4 and 5 demonstrate the eigenfrequencies for identical half-spaces and Tables 6 and 7 are for dissimilar media. The analysis confirms that the eigenfrequencies of uniformly partially closed delamination are situated further from the real axis compared with an open crack. The more general conclusion is that the larger the average value of spring stiffness in the SBC for delamination, the further the eigenfrequencies from the real axis $\text{Im} \hat{k} = 0$.

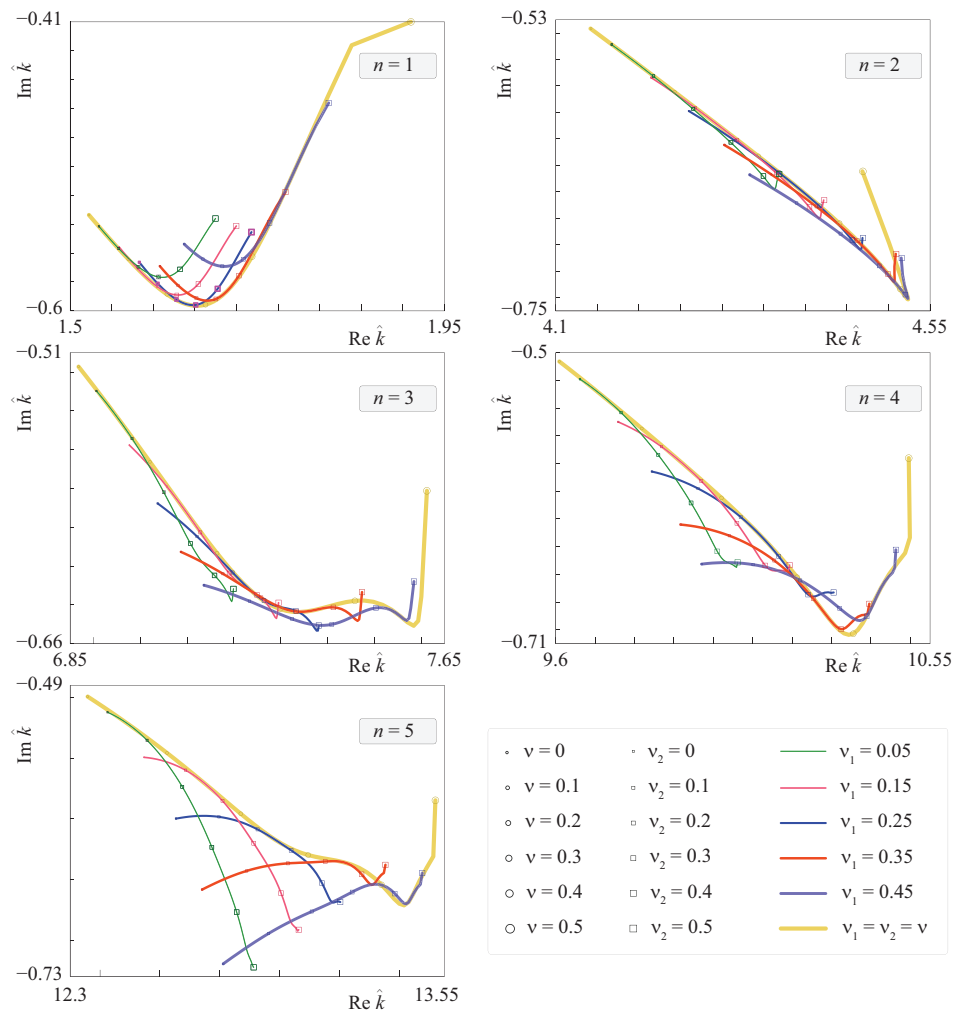


Figure 10. Eigenfrequencies $\hat{k}_n^0(v_1, v_2)$ for a circular crack between dissimilar elastic half-spaces; $\rho_1 = \rho_2, \mu_1 = \mu_2$.

Table 4. Eigenfrequencies \hat{k}_n^0 for open and bridged cracks in a homogeneous space (glass).

Eigenfrequency	Open Crack	Bridged Crack $\kappa^0 a/\hat{\mu} = 1$
\hat{k}_1^0	1.6392–0.5953 i	1.7466–0.64183 i
\hat{k}_2^0	4.3935–0.6578 i	4.6709–0.7432 i
\hat{k}_3^0	7.2317–0.6316 i	7.6603–0.7813 i
\hat{k}_4^0	10.1194–0.6319 i	10.6579–0.8931 i
\hat{k}_5^0	12.9837–0.6171 i	13.5403–0.9960 i

Table 5. Eigenfrequencies \hat{k}_n^0 for uniformly distributed and bridged delaminations in a homogeneous space (glass).

Eigenfrequency	Uniformly Partially Closed Delamination $\kappa^0 a/\hat{\mu} = 1$	Bridged Delamination $\kappa^0 a/\hat{\mu} = 1$ $\kappa^{\text{tip}} a/\hat{\mu} = 10$
\hat{k}_1^0	2.0584–1.4232 i	2.1573–1.5158 i
\hat{k}_2^0	4.8814–1.2382 i	5.1249–1.3648 i
\hat{k}_3^0	7.7694–1.0692 i	8.1361–1.2518 i
\hat{k}_4^0	10.7511–0.9727 i	11.2040–1.2551 i
\hat{k}_5^0	13.6850–0.9271 i	14.1255–1.3010 i

Table 6. Eigenfrequencies \hat{k}_n^0 for open and bridged cracks between aluminium and polycarbonate.

Eigenfrequency	Open Crack	Bridged Crack $\kappa^0 a/\hat{\mu} = 1$
\hat{k}_1^0	1.7906–0.6232 i	1.8574–0.6560 i
\hat{k}_2^0	4.4101–1.2778 i	4.5683–1.3788 i
\hat{k}_3^0	7.5124–0.8703 i	7.7492–0.9939 i
\hat{k}_4^0	10.3327–1.2528 i	10.6380–1.5031 i
\hat{k}_5^0	13.4210–0.9257 i	13.7657–1.1810 i

Table 7. Eigenfrequencies \hat{k}_n^0 for uniformly distributed and bridged delaminations between aluminium and polycarbonate.

Eigenfrequency	Uniformly Partially Closed Delamination $\kappa^0 a/\hat{\mu} = 1$	Bridged Delamination $\kappa^0 a/\hat{\mu} = 1$ $\kappa^{tip} a/\hat{\mu} = 10$
\hat{k}_1^0	2.1615–1.1530 i	2.2316–1.1970 i
\hat{k}_2^0	4.4559–1.7796 i	4.7643–2.0668 i
\hat{k}_3^0	7.7061–1.2261 i	8.0901–1.6362 i
\hat{k}_4^0	10.6059–1.7710 i	10.3337–2.3692 i
\hat{k}_5^0	13.8405–1.1542 i	14.2268–1.5495 i

The BIEM can also be employed for determining the resonance response of delaminations at the eigenfrequencies. Thus, Figure 11 exhibit the amplitudes of the non-zero vertical components of the COD $|\Delta u|$ corresponding to the resonance regimes of motion at the first five eigenfrequencies $\hat{k}_n^0, n = 1, 5$ given in Tables 6 and 7 for interface delaminations of the four considered kinds. An interesting conclusion can be made by analysing Figure 11: maximal amplitudes are achieved in the centre of circular delamination for open and bridged cracks, which are characterized by the stress-free boundary conditions in the centre ($\kappa^0 = 0$). On the other hand, the maximum values of the COD for uniformly partially closed and bridged delaminations with ($\kappa^0 \neq 0$) are reached further from the centre of Ω .

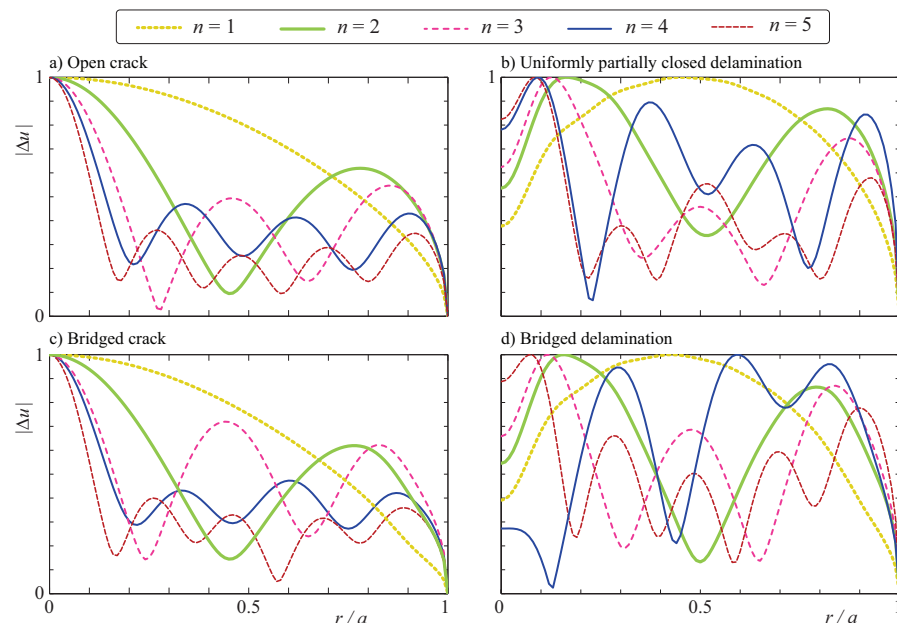


Figure 11. The amplitudes of the non-zero components of the COD $|\Delta u|$ corresponding to the resonance regimes of motion at the eigenfrequencies \hat{k}_n^0 for interface delaminations of four kinds: two half-spaces are made of aluminium and polycarbonate.

To give another example of the BIEM applicability for the solution of the problems of non-destructive evaluation, the amplitudes $|u_j(10^3, \theta = \pi/2 \pm \pi/2, \vartheta)|$ of the longitudinal and transverse waves scattered by each of the four circular delaminations is depicted

in Figure 12. Naturally, an open crack scatters more energy, so the amplitudes of the scattered wave-fields are the largest compared to the three other cases in most of the directions. Nevertheless, scattered transverse waves are larger for a uniformly partially closed delamination and a bridged delamination within sectors $25^\circ \leq \theta \leq 60^\circ$ and $134^\circ \leq \theta \leq 146^\circ$. Such a piece of information might be useful for the damage identification procedure, where the partially closed contact is taken into account.

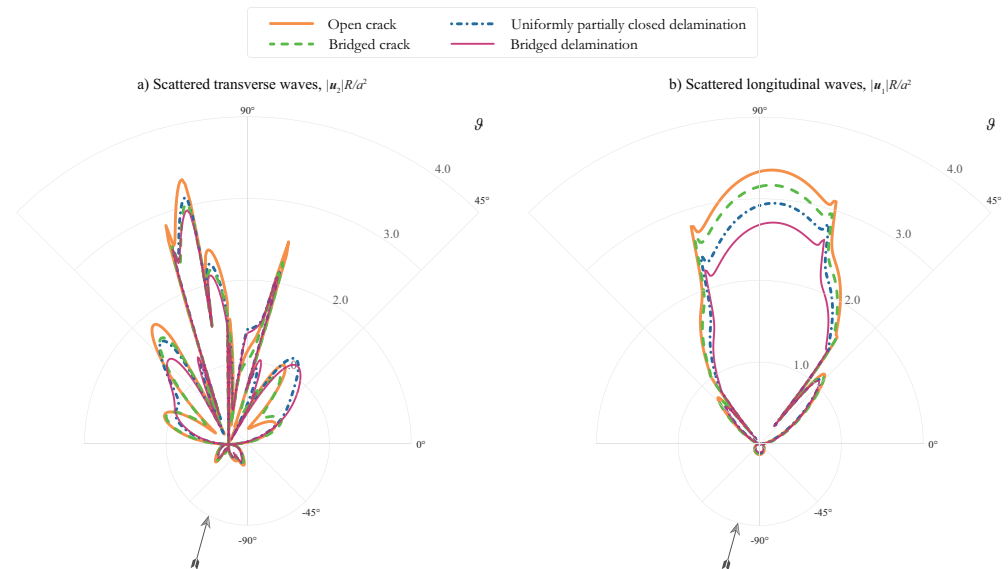


Figure 12. Amplitudes of the transverse $|u_2(10^3, \theta = \pi/2 \pm \pi/2, \theta)|$ (a) and longitudinal $|u_1(10^3, \theta = \pi/2 \pm \pi/2, \theta)|$ (b) waves scattered by a circular interface delamination for the transverse SV-wave incident at 15° angle to plane $x_3 = 0$ and 90° angle to plane $x_2 = 0$: two half-spaces are made of aluminium and polycarbonate, $k_{T2}a = 8$.

5. Discussion

The present paper demonstrates that the proposed BIEM is an efficient tool for the eigenfrequencies calculation and classification. The proposed advanced BIEM is more efficient for eigenfrequencies calculation than the meshless method and the finite element method, which demand more computational costs for the system composition and solution as well as eigenfrequencies determination. However, some limitations of the presented advanced BIEM should be also mentioned. At first, the presented BIEM is not suitable for elliptical interface delaminations, which are also often evaluated in practice. Also, the presented method cannot be easily extended for interface circular damages in anisotropic composites.

The authors believe that the proposed advanced BIEM will be useful for damage identification because each delamination has a unique set of the spectral points or resonance frequencies, which can be estimated from experimental data [4,5]. Besides, the introduction of the SBCs allows to distinguish and identify more kinds of delaminations.

Several extensions with applications in the nondestructive evaluation are also possible. Thus, in the presented BIEM formulation, the Hankel transforms of Green's matrices are constructed for two-layered media. The procedure can be naturally extended for multi-layered composites, where the SBCs can also be formulated at the internal boundaries, which allows simulating imperfect contact between sub-layers of a laminate due to adhesive degradation [23]. Another possible extension of the advanced BIEM is an extension for multiple circular delaminations (so-called impact-induced damage). For this purpose, multiple damages might be introduced in a laminate interfaces in the form of a set of delaminations, which will lead to the systems of the boundary integral equations for each delamination.

Author Contributions: Conceptualization, M.V.G. and O.V.D.; methodology, M.V.G. and O.V.D.; software, M.V.G.; validation, M.V.G. and O.V.D.; formal analysis, M.V.G. and O.V.D.; investigation, M.V.G. and O.V.D.; resources, M.V.G.; data curation, M.V.G.; writing—original draft preparation, M.V.G. and O.V.D.; writing—review and editing, M.V.G. and O.V.D.; visualization, M.V.G.; project administration, M.V.G. All authors have read and agreed to the published version of the manuscript.

Funding: This research was funded by the Ministry of Science and Higher Education of the Russian Federation (Project No FZEN-2020-0017).

Institutional Review Board Statement: Not applicable

Informed Consent Statement: Not applicable

Data Availability Statement: Data sharing not applicable to this article as no datasets were generated or analyzed during the current study.

Acknowledgments: The authors are grateful to E.V. Glushkov, N.V. Glushkova and A.A. Eremin for valuable and fruitful discussions.

Conflicts of Interest: The authors declare no conflict of interest.

References

- Überall, H.; Moser, P.; Murphy, J.; Nagl, A.; Igiri, G.; Subrahmanyam, J.; Gaunard, G.; Brill, D.; Delsanto, P.; Alemar, J.; Rosario, E. Electromagnetic and acoustic resonance scattering theory. *Wave Motion* **1983**, *5*, 307–329. [\[CrossRef\]](#)
- Singh, K.V. Transcendental inverse eigenvalue problems in damage parameter estimation. *Mech. Syst. Signal Process.* **2009**, *23*, 1870–1883. [\[CrossRef\]](#)
- Shifrin, E.; Lebedev, I. Identification of multiple cracks in a beam by natural frequencies. *Eur. J. Mech.-A Solids* **2020**, *84*, 104076. [\[CrossRef\]](#)
- Eremin, A.A.; Golub, M.V.; Glushkov, E.V.; Glushkova, N.V. Identification of delamination based on the Lamb wave scattering resonance frequencies. *NDT E Int.* **2019**, *103*, 145–153. [\[CrossRef\]](#)
- Solodov, I.; Bernhardt, Y.; Kreutzbruck, M. Resonant Airborne Acoustic Emission for Nondestructive Testing. *Appl. Sci.* **2021**, *11*, 141. [\[CrossRef\]](#)
- Ursell, F. Trapping modes in the theory of surface waves. *Math. Proc. Camb. Philos. Soc.* **1951**, *47*, 347–358. [\[CrossRef\]](#)
- Stocks, D.C. An experimental investigation of wave energy trapping. *Int. J. Eng. Sci.* **1976**, *14*, 947–962. [\[CrossRef\]](#)
- Aristegui, C.; Shuvalov, A.L.; Poncelet, O.; Caleap, M. Trapping of shear acoustic waves by a near-surface distribution of cavities. *J. Acoust. Soc. Am.* **2009**, *125*, 628–631. [\[CrossRef\]](#)
- Nazarov, S.A. Scheme for interpretation of approximately computed eigenvalues embedded in a continuous spectrum. *Comput. Math. Math. Phys.* **2013**, *53*, 702–720. [\[CrossRef\]](#)
- Pagneux, V. Trapped Modes and Edge Resonances in Acoustics and Elasticity. In *Dynamic Localization Phenomena in Elasticity, Acoustics and Electromagnetism*; Craster, R.V., Kaplunov, J., Eds.; Springer: Vienna, Austria, 2013; pp. 181–223. [\[CrossRef\]](#)
- Mishuris, G.S.; Movchan, A.B.; Slepyan, L.I. Waves in elastic bodies with discrete and continuous dynamic microstructure. *Philos. Trans. R. Soc. London Ser. A Math. Phys. Sci.* **2020**, *378*, 20190313. [\[CrossRef\]](#)
- Pao, Y.-H.; Mow, C.-C. *Diffraction of Elastic Waves and Dynamic Stress Concentrations*; Crane, Russack & Co. Inc.: New York, NY, USA, 1973; p. 696.
- Babich, V.M.; Kiselev, A.P. *Elastic Waves. A High-Frequency Theory*; BHV-Petersburg: St Petersburg, Russia, 2014; p. 320.
- Boyadzhiev, G. Bi-characteristic curves of body and surface waves and application in geophysics. *Serdica Math. J.* **2015**, *41*, 513–526.
- Manolis, G.D.; Dineva, P.S.; Rangelov, T.V.; Wuttke, F. State-of-the-Art for the BIEM. In *Seismic Wave Propagation in Non-Homogeneous Elastic Media by Boundary Elements. Solid Mechanics and Its Applications*; Springer: Cham, Switzerland, 2017; Volume 240. [\[CrossRef\]](#)
- Kitahara, M. *Boundary Integral Equation Methods in Eigenvalue Problems of Elastodynamics and Thin Plates*; Elsevier: Amsterdam, The Netherlands, 1985.
- Alves, C.J.S.; Antunes, P.R.S. Determination of elastic resonance frequencies and eigenmodes using the method of fundamental solutions. *Eng. Anal. Bound. Elem.* **2019**, *101*, 330–342. [\[CrossRef\]](#)
- Comninou, M. The Interface Crack. *J. Appl. Mech.* **1977**, *44*, 631–636. [\[CrossRef\]](#)
- Aleshin, V.; Delrue, S.; Trifonov, A.; Bou Matar, O.; Van Den Abele, K. Two dimensional modeling of elastic wave propagation in solids containing cracks with rough surfaces and friction—Part I: Theoretical background. *Ultrasonics* **2018**, *82*, 11–18. [\[CrossRef\]](#) [\[PubMed\]](#)
- Goldstein, R.; Perelmuter, M. An interface crack with non-linear bonds in a bridged zone. *J. Appl. Math. Mech.* **2011**, *75*, 106–118. [\[CrossRef\]](#)
- Rice, J.R.; Levy, N. The part-through surface crack in an elastic plate. *J. Appl. Mech.* **1972**, *39*, 185–194. doi: 10.1115/1.3422609. [\[CrossRef\]](#)

22. Baik, J.M.; Thompson, R.B. Ultrasonic scattering from imperfect interfaces: A quasi-static model. *J. Nondestruct. Eval.* **1984**, *4*, 177–196. [[CrossRef](#)]
23. Golub, M.V.; Doroshenko, O.V.; Wilde, M.V.; Eremin, A.A. Experimental validation of the applicability of effective spring boundary conditions for modelling damaged interfaces in laminate structures. *Compos. Struct.* **2021**, *273*, 114141. [[CrossRef](#)]
24. Martin, P.A.; Wickham, G. Diffraction of elastic waves by a penny-shaped crack: Analytical and numerical results. *Proc. R. Soc. Lond. Ser. A Math. Phys. Sci.* **1983**, *390*, 91–129. [[CrossRef](#)]
25. Neerhoff, F. Diffraction of Love waves by a stress-free crack of finite width in the plane interface of a layered composite. *Appl. Sci. Res.* **1979**, *35*, 265–315. [[CrossRef](#)]
26. Vatulyan, A.O.; Yurov, V.O. Numerical and Asymptotic Solution of the Problem of Oscillations of an Inhomogeneous Waveguide with an Annular Crack of Finite Width. *Acoust. Phys.* **2020**, *66*, 441–448. [[CrossRef](#)]
27. Mal, A. Interaction of elastic waves with a penny-shaped crack. *Int. J. Eng. Sci.* **1970**, *8*, 381–388. [[CrossRef](#)]
28. Krenk, S.; Schmidt, H. Elastic wave scattering by a circular crack. *Philos. Trans. R. Soc. London Ser. A Math. Phys. Sci.* **1982**, *308*, 167–198. [[CrossRef](#)]
29. Kundu, T.; Boström, A. Elastic wave scattering by a circular crack in a transversely isotropic solid. *J. Appl. Mech. Trans. ASME* **1991**, *58*, 695–702. [[CrossRef](#)]
30. Menshykov, O.V.; Menshykov, V.A.; Guz, I.A. Elastodynamics of a crack on the bimaterial interface. *Eng. Anal. Bound. Elem.* **2009**, *33*, 294–301. [[CrossRef](#)]
31. Lekesiz, H.; Katsube, N.; Rokhlin, S.I.; Seghi, R.R. The stress intensity factors for a periodic array of interacting coplanar penny-shaped cracks. *Int. J. Solids Struct.* **2013**, *50*, 186–200. [[CrossRef](#)] [[PubMed](#)]
32. Kanaun, S. Scattering of monochromatic elastic waves on a planar crack of arbitrary shape. *Wave Motion* **2014**, *51*, 360–381. [[CrossRef](#)]
33. Mykhas'kiv, V.; Stankevych, V.; Zhabdynskiy, I.; Zhang, C. 3-D dynamic interaction between a penny-shaped crack and a thin interlayer joining two elastic half-spaces. *Int. J. Fract.* **2009**, *159*, 137–149. [[CrossRef](#)]
34. Mykhas'kiv, V.; Zhabdynskiy, I.; Zhang, C. Dynamic stresses due to time-harmonic elastic wave incidence on doubly periodic array of penny-shaped cracks. *J. Math. Sci.* **2014**, *203*, 114–122. [[CrossRef](#)]
35. Golub, M.V.; Doroshenko, O.V.; Boström, A. Effective spring boundary conditions for a damaged interface between dissimilar media in three-dimensional case. *Int. J. Solids Struct.* **2016**, *81*, 141–150. [[CrossRef](#)]
36. Saha, T.; Roy, A. Weight function for an elliptic crack in an infinite medium-II. Shear loading. *Int. J. Fract.* **2001**, *112*, 1–21. [[CrossRef](#)]
37. Guan, L.; Norris, A. Elastic wave scattering by rectangular cracks. *Int. J. Solids Struct.* **1992**, *29*, 1549–1565. doi: 10.1016/0020-7683(92)90133-E. [[CrossRef](#)]
38. Glushkov, Y.V.; Glushkova, N.V. Resonant frequencies of the scattering of elastic waves by three-dimensional cracks. *J. Appl. Math. Mech.* **1998**, *62*, 803–806. [[CrossRef](#)]
39. Glushkov, Y.V.; Glushkova, N.V. Diffraction of elastic waves by three-dimensional cracks of arbitrary shape in a plane. *J. Appl. Math. Mech.* **1996**, *60*, 277–283. [[CrossRef](#)]
40. Eriksson, A.S. Natural Frequencies of a Penny-Shaped Crack With Spring Boundary Condition. *J. Appl. Mech.* **1995**, *62*, 59–63. [[CrossRef](#)]
41. Kaptsov, A.; Shifrin, E. The dynamics of an elliptical crack in an elastic space: Solution using Padé approximations. *J. Appl. Math. Mech.* **1991**, *55*, 416–423. [[CrossRef](#)]
42. Shpak, A.N.; Golub, M.V.; Mueller, I.; Eremin, A.A.; Kathol, J.; Fritzen, C.P. Influence of a delamination on Lamb wave excitation by a nearby piezoelectric transducer. *J. Intell. Mater. Syst. Struct.* **2021**, *32*, 267–283. [[CrossRef](#)]
43. Glushkov, E.; Glushkova, N.; Eremin, A. Forced wave propagation and energy distribution in anisotropic laminate composites. *J. Acoust. Soc. Am.* **2011**, *129*, 2923–2934. [[CrossRef](#)]
44. Sveshnikov, A.G. The limit absorption principle for a waveguide. *Dokl. Akad. Nauk USSR* **1951**, *80*, 345–347.
45. Boström, A.; Peterson, L. *Wave Scattering by a Circular Crack in the Interface between Two Elastic Media*; Technical Report, Report 1989:7; Division of Mechanics, Chalmers University of Technology: Goteburg, Sweden, 1989.
46. Glushkov, E.V.; Glushkova, N.V.; Ekhlakov, A.V. A mathematical model of the ultrasonic detection of three-dimensional cracks. *J. Appl. Math. Mech.* **2002**, *66*, 141–149. [[CrossRef](#)]
47. Sidorov, Y.V.; Fedoryuk, M.V.; Shabunin, M.I. *Lectures on the Theory of Functions of a Complex Variable*; Mir Publishers: Moscow, Russia, 1985.
48. Prudnikov, A.P.; Brychkov, Y.A.; Marichev, O.I. *Integrals and Series. Volume 3: More Special Functions*; Gordon and Breach Science Publishers: London, UK 1989; p. 800.
49. Golub, M.V.; Doroshenko, O.V. Effective spring boundary conditions for modelling wave transmission through a composite with a random distribution of interface circular cracks. *Int. J. Solids Struct.* **2019**, *165*, 115–126. doi: 10.1016/j.ijsolstr.2019.02.002. [[CrossRef](#)]
50. Golub, M.V.; Doroshenko, O.V. Effective spring boundary conditions modelling wave scattering by an interface with a random distribution of aligned interface rectangular cracks. *Eur. J. Mech.-A Solids* **2020**, *81*, 103894. [[CrossRef](#)]
51. Perelmuter, M. Analysis of interaction of bridged cracks and weak interfaces. *Int. J. Mech. Sci.* **2018**, *149*, 349–360. [[CrossRef](#)]